Unclassified

TBD 1994

Investigations Pertaining to the Implementation of an Interferometer Sounder on Geostationary Satellites

Professor William L. Smith

Prepared for
Massachusetts Insitute of Technology
Lincoln Laboratory
244 Wood Street
Post Office Box 73
Lexington, MA 02173-9108

Under Purchase Order BX-5125
Prime Contract F19628-90-C-0002

Distribution statement (TBD)

Prepared by
Cooperative Institute for Meteorological Satellite Studies
(CIMSS)
Space Science and Engineering Center (SSEC)
at the University of Wisconsin-Madison
1225 West Dayton Street
Madison, WI 53706

Unclassified

INVESTIGATIONS PERTAINING TO THE IMPLEMENTATION OF AN INTERFEROMETER SOUNDER ON GEOSTATIONARY SATELLITES

Background

The GOES High Resolution Interferometer Sounder, (Smith et al., 1990), GHIS has been designed for flight on future geostationary meteorological satellites. Airborne applications of an aircraft prototype instrument (the University of Wisconsin HIS which flies on the NASA high altitude ER-2 aircraft) have demonstrated that large improvements in temperature and water vapor vertical resolution and profile accuracy can be achieved with a High spectral resolution Interferometer Sounder (HIS) in place of the broader spectral interval filter radiometers now used on the GOES satellites. One practical approach for implementing the GOES-HIS is to modify the existing GOES I/M filter wheel sounder by replacing an interferometer module in place of the filter wheel assembly, leaving the telescope and detector-cooler assemblies essentially unchanged. A NOAA funded feasibility study was successfully concluded by a team comprised of University of Wisconsin, ITT, and Hughes-SBRC personnel. However, implementation of the approach had been on hold until resolution of problems with the GOES/I spacecraft and filter instruments. With those problems resolved, NOAA charged the MIT Lincoln Laboratory to perform an engineering study of the GHIS as an initial step towards ultimate implementation of the approach on GOES N or N'. An important basis for the MIT/LL study is the trade-off between sounding performance and instrument NEΔN. Since the CIMSS is ideally suited to perform the retrieval simulations needed to define this particular trade-off, MIT/LL supported this study through a subcontract.

The study reported here consisted of simulating both GHIS and GOES filter instrument radiances for one hundred temperature and water vapor profiles selected from the well known "Phillips Sounding Data Set". The data set is that used by the EOS-AIRS (Atmospheric InfraRed Sounder) Science team for testing algorithms developed for that instrument. The 100 profiles range between the extreme meteorological conditions found around the globe throughout an entire year. A fast transmittance model, needed for calculating both GHIS and the GOES-I filter radiometer radiance "measurements," was developed as part of this contract and is described in Appendix A. Complete non-linear physical retrievals

were performed using the retrieval methodology described in Appendix B. The fast transmittance model, described in appendix A, was also used to calculate the weighting functions needed for the physical profile retrieval process.

Results

As noted above, radiance simulations and profile retrievals were performed for 100 profiles representing the complete range of air mass characteristics observed over the globe. Four levels of instrument noise were considered corresponding to four levels of noise associated with spatial averaging to be used to cope with cloudiness, and/or relative detection performance; (a) 100 km resolution (1/10 single sample noise), (b) 50 km resolution (1/5 single sample noise), (c) condition (b) with 50% discarded (e.g. due to cloudiness), and (d) condition (b) with 90% discarded (e.g., 90% cloud cover). The single sample noise levels assumed for the GOES-I filter radiometer and for GHIS are provided in Table I. For GOES-I, the single sample noise values are those achieved during thermal vacuum tests for a 100 msec total dwell time per sounding and provided by Dr. W. Paul Menzel of NOAA. The GHIS single sample noise values are those estimated by MIT/LL for a 400 msec dwell time per sounding as based on GOES-I detector performance and the GHIS design. Since the GOES-I sounding time is one-fourth that of the GHIS, the noise factor for GOES-I is one-half that of GHIS (i.e., detector signal to noise increases with the square root of the dwell time). The NEΔT values for all GHIS spectral channels are achieved by linear interpolation of the values shown in Table I. The spectral resolution (unapodized) adopted for the GHIS simulations was 0.632 cm^{-1}, 1.264 cm^{-1}, and 2.528 cm^{-1} for the longwave, midwave, and shortwave bands respectively. Theoretical studies show that this spectral resolution is sufficient for achieving the full benefit of a high spectral resolution sounder. It should be noted that the adopted spectral resolutions for this study are equivalent to those of the original GHIS design (Smith et al., 1990) for the medium spectral resolution mode. The longwave and midwave bands (0.625 cm^{-1} and 1.25 cm^{-1}, unapodized, respectively) are practically the same as the original design but the shortwave bands differ by nearly a factor of two (i.e., 2.5 cm^{-1}, assumed here, as opposed to 1.15 assumed for the original GHIS design). Although the shortwave channel spectral resolution differences impact the NEΔT performance of the GHIS design, they

have little influence on the weighting functions (i.e., the profile sensitivity of the various spectral channels) which impact the profile retrieval vertical resolution and accuracy.

Although the GHIS NEΔT performance given in Table I seems large, it is important to note that these are generally superior to the GOES-I in terms of total energy noise (i.e., NEΔT times $\Delta\upsilon$), particularly for the longwave and midwave bands. As will be shown, this improved performance coupled with the much larger number of spectral channels and improved vertical resolution resulting from narrower spectral bands leads to greatly improved sounding performance.

Table I: Nominal single sample brightness temperature noise (at 250°K) for the GOES-I filter sounder and for a selection of "reference" GHIS channels.

GOES-I			GHIS		
υ_0	$\Delta\upsilon$	NEΔT	υ_0	$\Delta\upsilon$	NEΔT
680	13	0.81	620	0.63	1.63
696	13	0.62	753	0.63	1.07
711	13	0.52	885	0.63	1.36
733	16	0.42	1018	0.63	1.89
748	30	0.39	1150	1.25	2.78
790	50	0.20	1210	1.25	0.59
832	50	0.13	1343	1.25	0.90
907	25	0.10	1475	1.25	1.43
1030	25	0.15	1608	1.25	2.36
1345	55	0.17	1740	1.25	3.97
1425	80	0.18	2150	2.50	0.91
1535	60	0.40	2293	2.50	1.67
2188	23	0.42	2436	2.50	3.16
2210	23	0.35	2578	2.50	6.06
2245	23	0.43	2721	2.50	11.76
2420	40	0.37			
2513	40	0.61			
2671	100	0.47			

Experience has shown that sources of noise, independent of the instrument, impact the profile retrieval. This noise, commonly referred to as "Forward Model Noise," results from the fact that there are errors in spectroscopy (i.e., line strengths, widths and shape approximations used to specify atmospheric transmission), neglected constituents (i.e., aerosols, subvisible clouds, etc.), numerical quadrature errors, and other unaccounted for radiative effects (e.g., nonunity surface emissivity, scattering, etc.) which cause discrepancies between observed and calculated radiances. Experience with both aircraft and ground-based HIS data comparisons with theoretical calculations suggest that this "Forward Model Noise" is at a level of 0.2° K or greater, depending on spectral region and atmospheric condition. Thus, in this study we assumed a random forward model noise of 0.2° K.

The total noise influencing the retrieval process, in terms of NEΔT, is then

$$\epsilon_T = \sqrt{\epsilon_I^2 + 0.04}$$

where $\in_I$ is the instrument brightness temperature noise given by,
$\in_I = \in_{250K} * (\partial B/\partial T)_{T=250K} / (\partial B/\partial T)_{T=T_B}$, where B is Planck radiance and T is temperature, and 0.04 represents the random forward model noise variance. The purpose of this transformation is to retrieve the original noise specification which was listed in terms of an NEΔT for a scene temperature of 250°K. A computer random number generator is used to produce individual errors selected from a Guassian distribution with a standard deviation of $\in_T$ which are then added to the calculated radiances to simulate real observations.

The retrieval error statistics are presented as a function of vertical resolution in order to assess the trade-off between retrieval accuracy and vertical resolution. This is achieved by vertically averaging the individual level retrieval errors over layers of varying thickness prior to computing the root mean square difference (RMSE) over the one hundred profile data set. Linear interpolation is used to obtain a precise estimate of the error for layers of a given thickness surrounding each retrieval level.

Table II provides a statistical summary of the profile retrieval errors for six different profile vertical resolutions and four different instrument noise conditions. An inspection of these results reveal that:

(1) The improvement of GHIS over the GOES filter radiometer is more dramatic for temperature than for dewpoint. This result is probably due to the great difficulty of retrieving water vapor from radiance measurements due to the high degree of nonlinearity in the inverse solution. We believe that the current retrieval methodology is not yet optimal for exploiting the full benefit of GHIS with regards to achieving a convergent solution for the water vapor profile. An improved algorithm should enable the use of many more water vapor channel radiances and this should yield much higher water vapor profile accuracy than is demonstrated here.

(2) For 1/5 nominal instrument performance (i.e., the cloudfree 50 km sounding resolution condition) and a practical vertical resolution of 2 km, the GHIS achieves the desired 1^{o} K temperature profile accuracy and 2.3^{o} K dewpoint temperature profile accuracy. The GOES filter radiometer profile retrieval error is 50% greater than the GHIS retrieval error at this resolution. It is also revealing to note that the GHIS accuracy improves almost in proportion to the square root of the layer thickness (beyond 1 km) indicating that the GHIS temperature profile errors are relatively uncorrelated vertically for resolutions

below 1 km. The GOES retrieval errors, however, decreases much more slowly with layer thickness revealing a stronger vertical correlation of the retrieval error indicative of poorer vertical resolution. In fact it can be seen for temperature that the accuracy of GOES derived four kilometer layer average temperatures is equivalent to that of GHIS 1 - 2 km layer average values indicating that GHIS possesses more than twice the vertical resolution of GOES-I. For water vapor, the vertical resolution advantage of GHIS appears smaller (i.e., about 1.5 : 1) but this is believed to be due to the water vapor retrieval limitations discussed earlier.

Figure 1 shows a summary of the variation of temperature profile retrieval error for different vertical resolution as a function of instrumental noise. Comparison of GHIS with GOES-I reveals that significant reductions of noise (e.g., due to improved detector performance) would have little impact on the improvement of the low spectral resolution GOES-I sounding performance but would have significant impact on the sounding accuracy of GHIS which is already a factor of two better than GOES-I. This performance sensitivity to detector noise characteristically is due to the large difference in the number of spectral channels between GHIS and GOES-I. Figures 2 shows profiles of the temperature RMS error for GOES and GHIS which reveal the vertical dependence of the retrieval errors at various vertical resolutions. It can be seen that from figure 3, at two kilometer resolution and for nominal noise, the GHIS achieves about $1^{o}K$ accuracy throughout most of the atmosphere (100 - 1000 hPa). The largest improvements of GHIS over GOES occur in the tropopause region 100 - 300 mb where the sharp changes in lapse rate are much better resolved by the interferometer than by the filter radiometer. Figure 3b, for water vapor, reveals that the biggest improvement of GHIS over the GOES filter radiometer is in the thermodynamically important middle troposphere. Figure 4 shows an example of a GHIS and a GOES filter radiometer retrieval randomly selected from the independent sample of cases used for this study. Although the vertical structure improvements appear to be small they are highly meteorologically significant, especially in terms of the implied atmospheric stability of the lower troposphere which determines the atmospheres tendency for convective storm development.

TEMPERATURE RMSE (Degree K) (100-1000 hPa)

Noise Factor	CØ (1/10)		C1 (1/5)		C2 (1/3.5)		C3 (1/1.6)	
Vertical Resolution (km)	GHIS (0.1)	GOES (0.05)	GHIS (0.2)	GOES (0.1)	GHIS (0.2857)	GOES (0.14285)	GHIS (0.625)	GOES (0.3125)
0	1.37	2.07	1.56	2.09	1.66	2.10	1.90	2.22
1	1.05	1.77	1.25	1.78	1.35	1.80	1.58	1.92
2	0.81	1.50	0.99	1.52	1.08	1.54	1.32	1.67
3	0.63	1.27	0.80	1.28	0.89	1.30	1.11	1.42
4	0.52	1.13	0.64	1.14	0.71	1.16	0.93	1.27
5	0.46	0.96	0.55	0.97	0.61	0.99	0.80	1.09

DEW POINT TEMPERATURE RMSE (degree K) (300-1000 hPa)

Noise Factor	CØ		C1		C2		C3	
Vertical Resolution (km)	GHIS	GOES	GHIS	GOES	GHIS	GOES	GHIS	GOES
0	3.02	3.48	3.18	3.49	3.21	3.49	3.55	3.50
1	2.56	3.05	2.73	3.05	2.83	3.05	3.13	3.07
2	2.17	2.70	2.33	2.70	2.44	2.71	2.74	2.72
3	1.89	2.37	2.04	2.37	2.13	2.37	2.44	2.39
4	1.68	2.11	1.81	2.11	1.90	2.11	2.18	2.13
5	1.55	1.91	1.66	1.91	1.73	1.91	1.99	1.93

Table II: Root Mean Square Errors (RMSE) of retrieved temperatures and dewpoints within the 100-1000 hectapascal layer of the atmosphere. The RMSE's are presented as a function of instrument noise and vertical resolution.

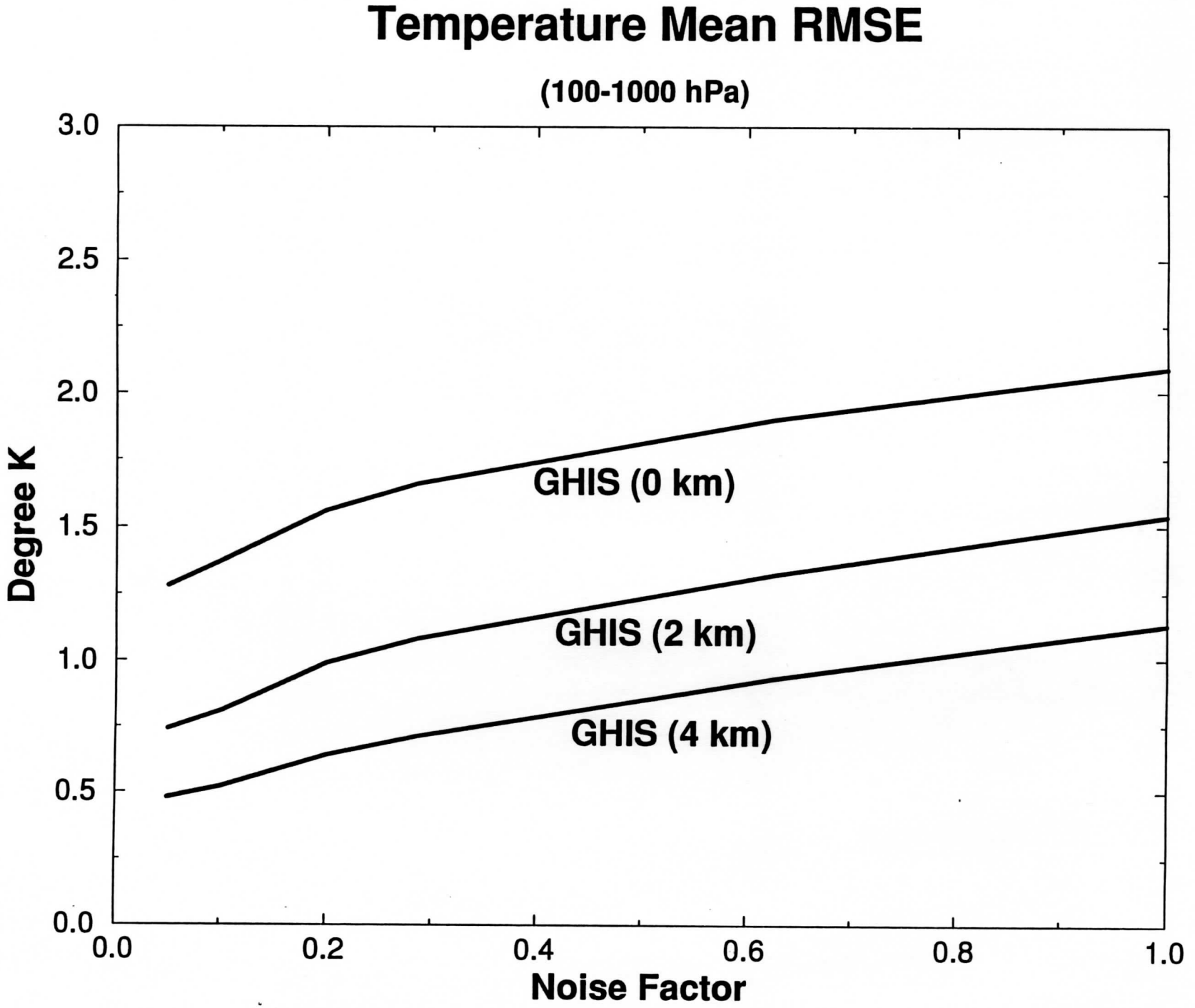

Figure 1a: Temperature retrieval RMSE's for GHIS at various vertical resolutions as a function of instrument noise

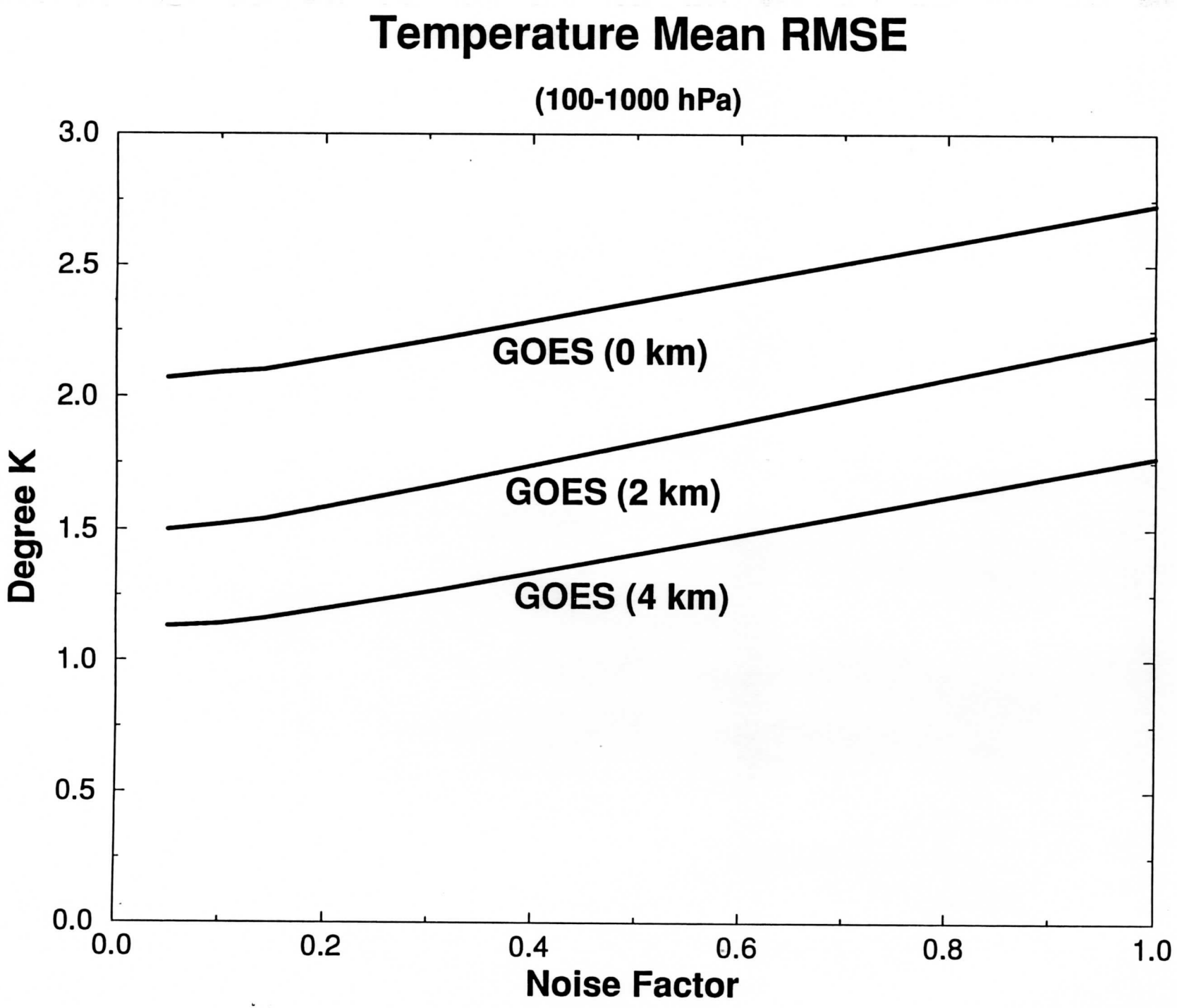

Figure 1b: Same as **1a** but for GOES filter sounder.

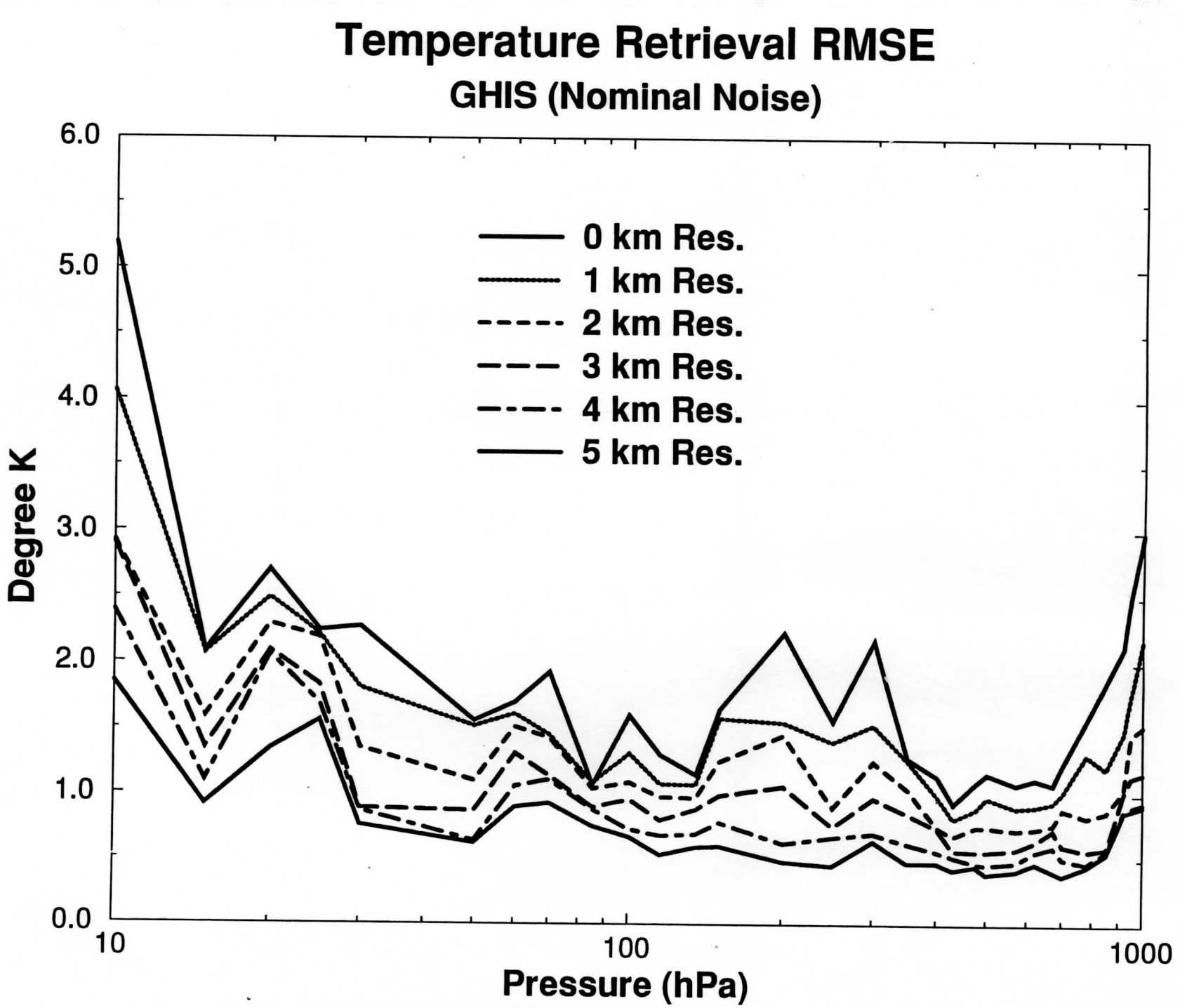

Figure 2a: GHIS temperature retrieval RMSE as a function of vertical resolution for nominal noise (noise condition C2).

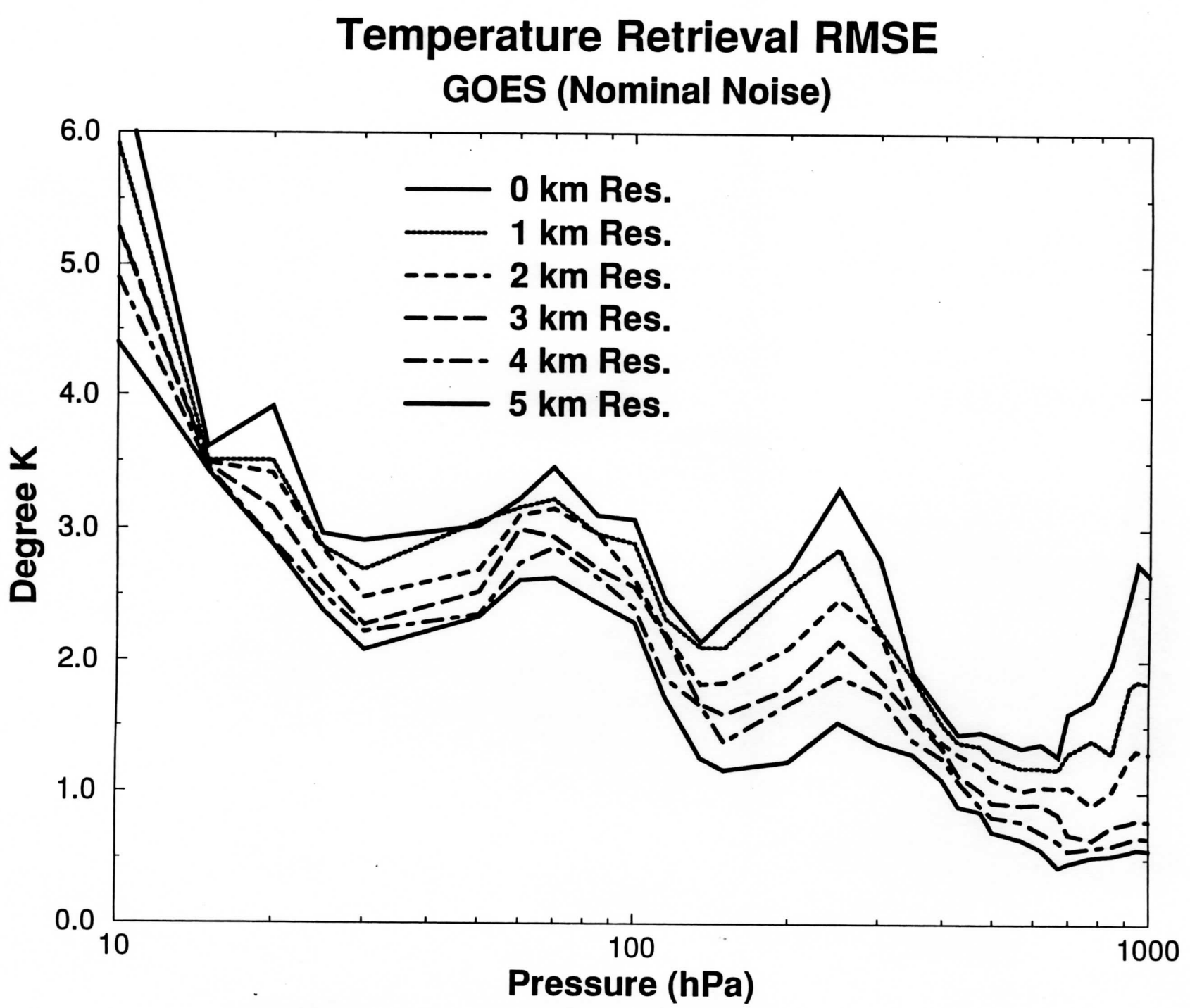

Figure 2b: Same as **2a** but for GOES filter radiometer.

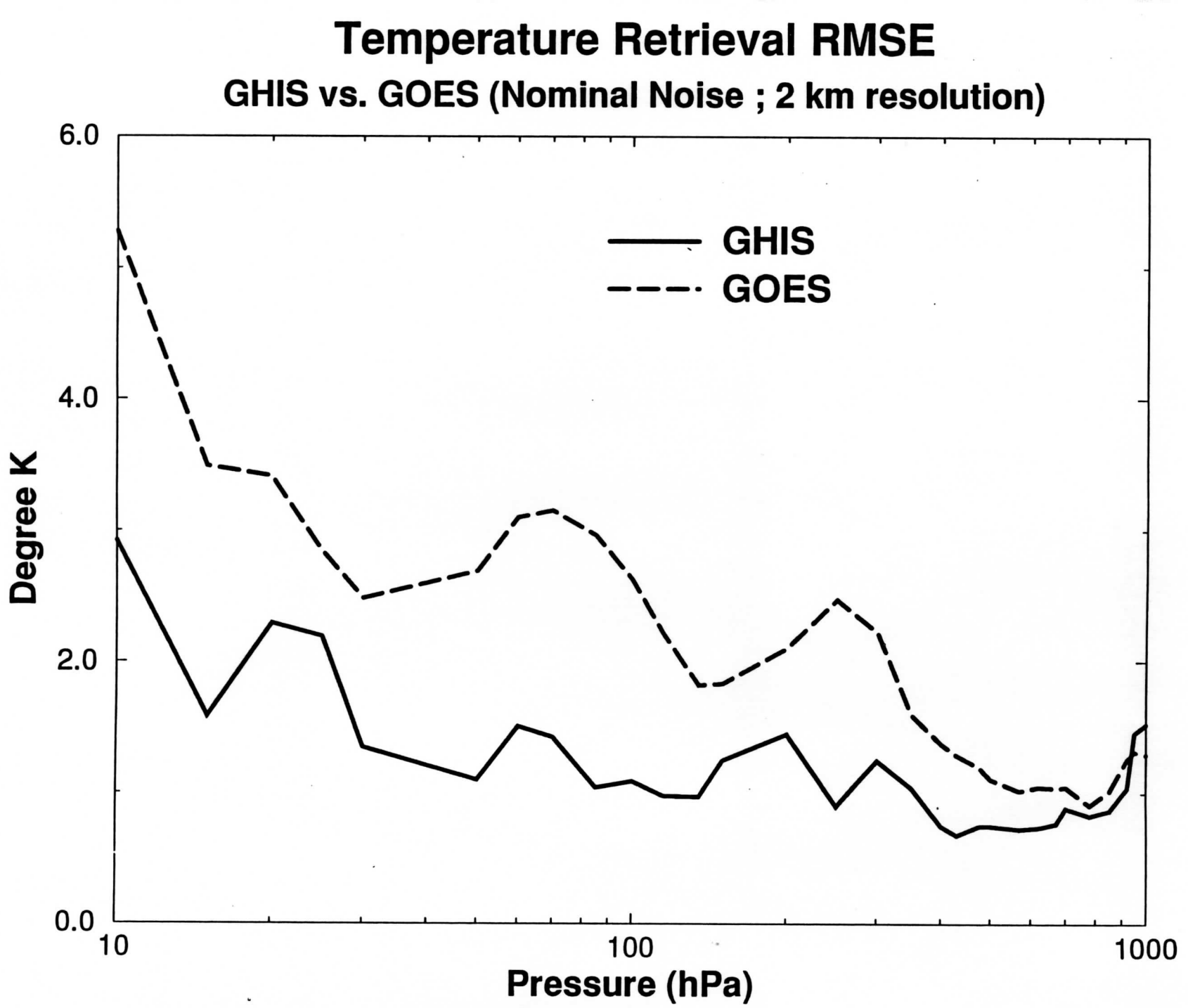

Figure 3a: Comparison of GHIS and GOES filter radiometer temperature profile errors for nominal noise (noise condition C2) and a 2 kilometer vertical resolution.

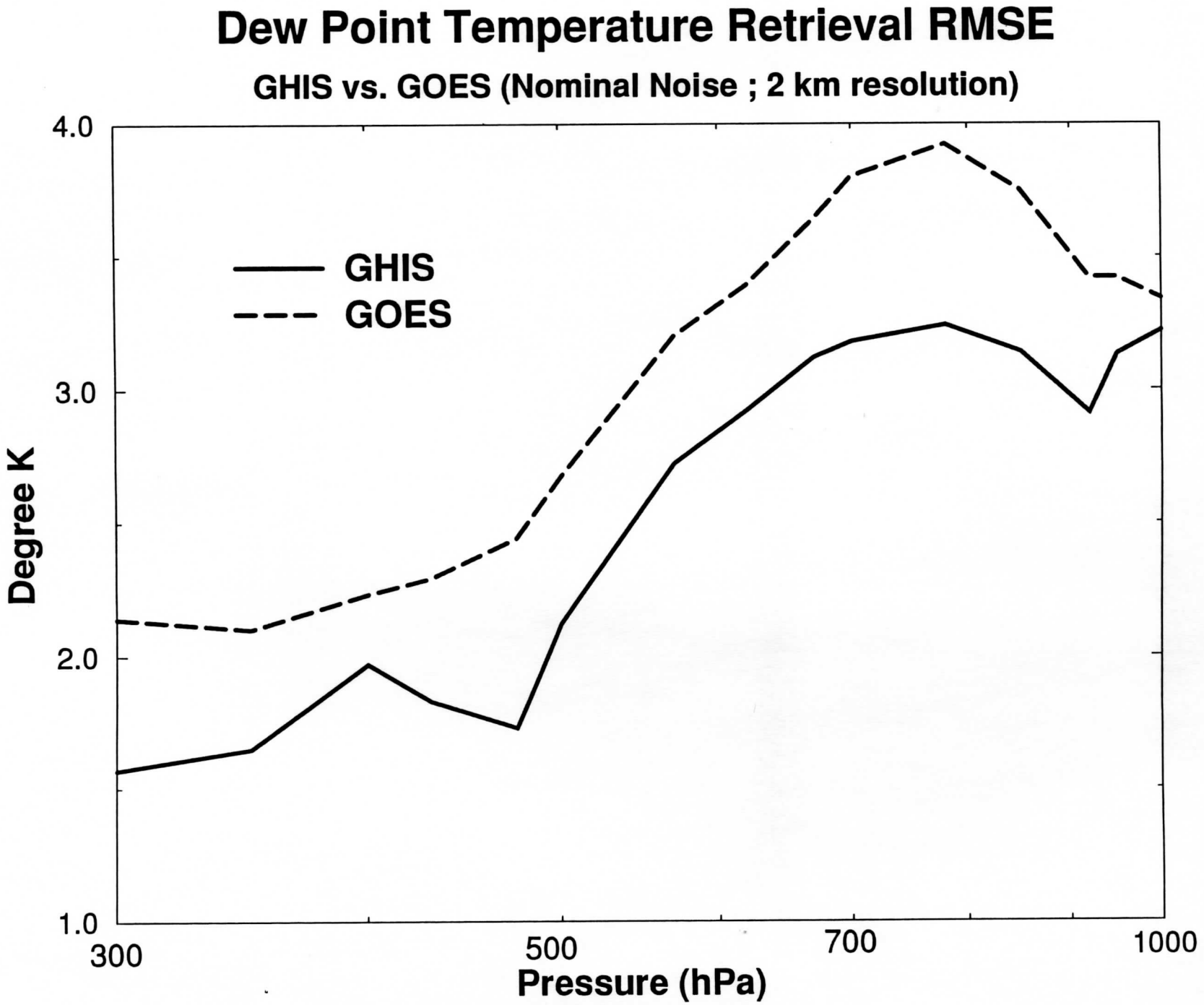

Figure 3b: Same as **3a** but for dewpoint temperature.

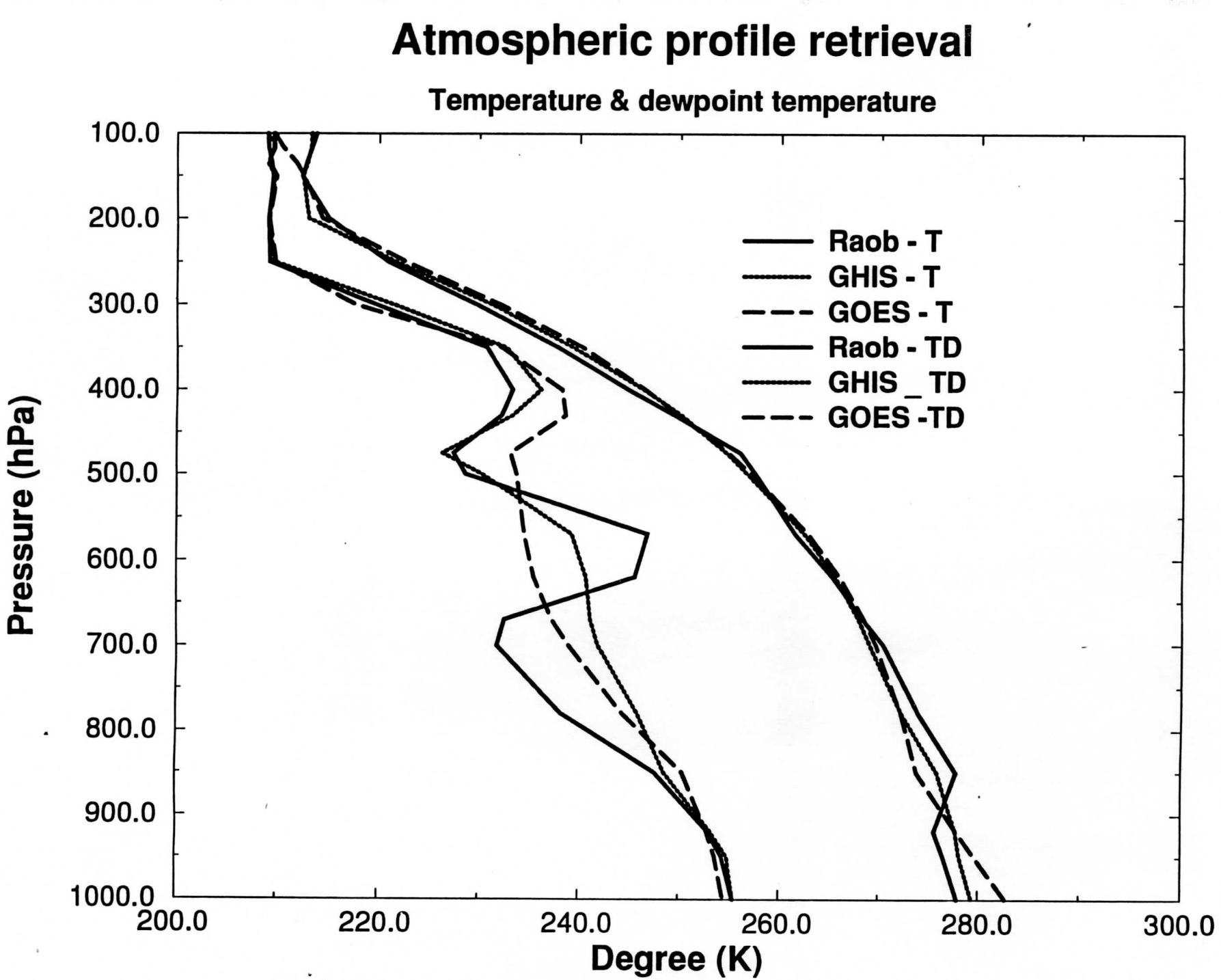

Figure 4: An example comparison of GHIS and GOES filter radiometer temperature and dewpoint temperature retrievals as compared to the radiosonde used to simulate the radiance observations for each instrument.

Additional Considerations

The ultimate GHIS performance will depend upon a number of instrument characteristics and operating scenarios. The GHIS will possess the spectral resolution and single sample noise characteristics which enable unprecedented vertical resolution and thermal accuracy to be achieved from geostationary satellites. An important advantage of GHIS over the current GOES-I sounder is that significant improvements in sounding performance can be achieved by reductions of measurement noise (i.e., through improved detector performance, greater space and time integration, etc.) This is not the case with the GOES filter radiometer which is already near the limit of performance indicated by the spectral characteristics of that instrument. A key advantage of the 3-axis stabilized GOES satellite, which will accommodate the GHIS, is that trade-offs between spectral resolution (i.e., vertical resolution), horizontal resolution, spatial coverage, time frequency, and radiometric accuracy can be performed in real time in order to optimize the sounding product for its intended application. This optimization can be implemented through the uploading of command sequences as is routinely performed with the current GOES-VAS system. Once the single sample noise characteristics of GHIS are defined, the results provided in this study can be used to provide definitive profile retrieval characteristics (i.e., vertical resolution and accuracy) for different intended operating scenarios.

References

Smith, W. L., H. E. Revercomb et al., 1993: GHIS-The GOES High-Resolution Interferometer Sounder. J. of Appl. Meteor., Vol 29, No. 12.

Appendix A: Construction of "fast" transmittance models for GHIS and GOES/I

1. Line-by-line database

Calculations have been done, using FASCOD3P and HITRAN92, for a set of 32 atmospheres, consisting of the 1976 U.S. Standard and 31 diverse profiles representing a wide range of meteorological conditions, from arctic to tropical. The very high, variable spectral resolution output was standardized to 0.1 cm**-1 by simple averaging. Three runs were made: "all", using the seven standard molecular species defined in FASCOD3P -- water vapor, carbon dioxide, ozone, nitrous oxide, carbon monoxide, and methane; "bwv", all of the preceding but water vapor; and "dry", defined as "bwv" without ozone. Division of "all" by "bwv" yields "wet", while the ratio of "bwv" and "dry" produces "ozo". By defining "wet" and "ozo" in this manner, the product rule for total transmittance is still valid, even though the 0.1-cm**-1 data are no longer representative of monochromatic radiation. The calculations span the spectral range 550 to 2950 cm**-1; the volume of the dataset is on the order of 600 Megabytes. For the present application, only nadir-viewing computations have been done. All calculations will be repeated for four additional zenith angles , producing a total data volume of 1.8 Gigabytes.

2. Preparation of data for generation of fast models

a. GHIS

The 0.1-cm**-1 data, which are incompletely sampled in the Nyquist sense, were converted to a completely sampled 0.2-cm**-1 resolution database by averaging adjacent points to yield values at an interval of 0.1-cm**-1 with a resolution of 0.2 cm**-1. The data were then grouped into three bands, each 8192 points in length: 550 - 1369, 1150 - 1969, and 1950 - 2769 cm**-1. Treating the transmittance at each level as a spectrum, FFT's were performed with an effective Nyquist wavenumber of 819.2 cm**-1, a delay spacing of 6.10351x10**-4 cm, and a maximum delay of 5 cm. The resulting interferograms were then divided by the sinc function to remove the effect of the previous boxcar convolution, and truncated at appropriate points, producing interferograms with the following properties:

Band	points	max delay	unapodized resolution
1	4096	2.50 cm	0.2 cm**-1
2	2048	1.25	0.4
3	2048	1.25	0.4

For current GHIS specifications, these were further reduced in volume as follows:

Band	points	delay(cm)	delta-wn(cm**-1)
1	1296	0.7910	0.632
2	648	0.3955	1.264
3	324	0.1977	2.528

This final set of interferograms were then FFT'ed back to spectra, and the spectra reorganized into transmittance profiles.

b. GOES/I

For this instrument, and for filter radiometers in general, postprocessing of the 0.1-cm**-1 line-by-line data is simple and straightforward. Again treating the transmittance at each level as a spectrum over the domain, convolution is performed between that spectrum and the spectral response function for each band or channel of the instrument, which has also been defined at the 0.1-cm**-1 interval. The results are then reorganized into profiles.

3. Fast models

For the instruments of immediate concern, as well as several others, so-called "fast", or "parameterized", or "regression" models have been and/or are being developed using the algorithm described by J.Eyre of the European Centre for Medium-range Weather Forecasting (ECMWF). Comparisons of Fast model radiance calculations with full Fascode 3P radiance calculations and with actual aricraft HIS radiance observations indicate that accuracies of the Fast model are comparable to the accuracy of the full Fascode 3P computation program for most spectral regions of the GHIS.

Bibliography

Clough, S. A., F. Kneizys, E. Shettle, 1986: Atmospheric Radiance and Transmittance: FASCOD2. Proc. Sixth Conference on Atmospheric Radiation.

Eyre, J. R., 1991: A fast radiative transfer model for satellite sounding systems. ECMWF Tech Memo 176.

Appendix B: Retrieval Procedures

CIMSS's atmospheric sounding retrieval system, can be described as a two step process; statistical regression followed by a physical nonlinear interative retrieval. The first step utilizes "least square regression" where the solution coefficients are calculated "off-line" from a quality controlled data base. The solution coefficients are the least square regression coefficients between profile vectors (temperature; water vapor and surface skin temperature) and their corresponding spectral channel brightness temperatures. The data base used here includes profiles from four seasons and over all latitude zones so that its universal characteristics can accomodate measurements from any kind of observational condition. These regression profiles are then used as an initial profile in a nonlinear iterative physical retrieval process. The data base selected in this study for the regression analysis is the 1761 TOVS Initial Guess Retrieval (TIGR) profiles (Chedin et al., 1985). One hundred profiles are selected from 1600 Phillip's sounding data set (Phillips et al., 1984) for the calculation of radiance spectra used for the profile retrieval simulations.

Profiles obtained by regression retrieval are not perfect since they result from a linear operator. This is especially true for the water vapor profile which is a highly nonlinear function of the radiance measurements. Mathematically, the nonlinear nature of the inverse solution of the radiative transfer equation for temperature and water vapor profiles results from the fact so called "Weighting Functions" required to obtain the inverse solution, depend on the unknown temperature and water vapor variables. This nonlinearity is weak for temperature but very strong for water vapor. As a consequence, satisfactory solutions for water vapor can only be achieved by a nonlinear iterative process. Thus, the second step nonlinear iterative simultaneous temperature and water vapor retrieval is designed to further refine the regression retrieval. The procedures given below are used in this study for profile retrieval from measurements simulated for clear conditions.

Since the radiance inversion problem is mathematically ill-posed, the smaller the number of unknowns to be calculated in an inversion solution the more stable the retrieval and the more efficient the computation. By following (Smith and Woolf, 1976) the profiles are mapped into a relatively small set of empirical orthogonal functions (EOFs) (or eigenvectors) where the coefficients of EOFs are to be retrieved.

The retrieval coefficients A, of the EOFs; written in the form of the maximum likelihood solution (Rodgers, 1976), is defined as

$$A_{n+1} = (K_n^T E^{-1} K_n + \gamma V^{-1})^{-1} K_n^T E^{-1} (\delta Y_n + K_n A_n) \qquad (1)$$

where the final $(n+1)$ *state vector* $x_{n+1} = X_o + \Phi A_{n+1}$.

In the above, Φ is the matrix of empirical orthogonal functions of the TIGR data set

$A = (\alpha_1, \alpha_2, ---\alpha_m)$; where the $\alpha' s$ are the coefficients of the empirical orthogonal functions

and $X = (T_1, T_2, --T_{n1}, ---\ln q_2, --\ln q_{n1}, Ts)^T$. In the above,

X_o = guess state of X,

$(\ )^T$ = matrix transpose,

$\delta X = X_n - X_o = \Phi A$,

E = Measurement error covariance matrix,

V = Covariance of A,

γ = Lagrangian multiplier,

$\delta y_n = T_B - T_{Bn}$ (T_B: brightness temperature),

$K_n^{'} = W_T^{(n)}; W_q^{(n)}$ and $W_{Ts}^{(n)}$,

$K_n = K_n^{'} \Phi$,

and the weighting functions $W_T; W_q$ and W_{Ts} are;

$$W_{Ts} = \beta_s \tau_s,$$

$$W_T = \beta d\tau,$$

$$Wq = (Ts - Ta)\, \tau_s \beta_s d\ln \tau_w,$$

where $\beta = \left(\partial B / \partial T\right)_{T = 250K} \Big/ \left(\partial B / \partial T\right)_{T = T_B}$.

Also, τ_w = water vapor transmittance,

τ = total transmittance,

Ts = surface skin temperature,

Ta = surface air temperature,

B = Planck radiance

Fourteen EOFs are choosen for the retrieval (9 EOFs for temperature and 5 EOF for water vapor). This number of EOFs was found to be optimal in the sense that it is small enough that a stable solution can be found for all profile conditions (so that all 100 profile retrievals are included in the statistics,) but large enough so that the total profile information content of the radiance spectra are extracted. The spectral

channels of GHIS used here for profile retrieval are selected using an analysis of the weighting functions designed to optimize the retrieval process in terms of computational efficiency. Only spectral channels which have significant sensitivity to the temperature and water vapor profile structure and for which the level of peak sensitivity is relatively independent of profile condition are selected for the retrieval process. For this study three hundred and forty eight GHIS channels and eighteen GOES channels are used in all steps of the retrieval as described above.

The single sample instrument noise for GHIS was specified by MIT Lincoln Laboratory (Kerekes, private communication) and presented in terms of brightness temperature noise at a set of reference frequencies at a reference temperature of 250K.

Table III: GHIS NEΔT values for a set of reference frequencies

cm^{-1}	K	cm^{-1}	K	cm^{-1}	K
620	1.63	1210	0.59	2150	0.91
753	1.07	1343	0.90	2293	1.67
885	1.36	1475	1.43	2436	3.16
1018	1.89	1608	2.36	2578	6.06
1150	2.78	1740	3.97	2721	11.76

Noise values for all other GHIS spectral frequencies are obtained by linear interpolation of the above values to the frequencies listed in Table IV.

The radiance noise, ϵ_I, is computed using

$$\epsilon_I = \epsilon_T \left(\frac{\partial B}{\partial T} \right)_{T=T_B}$$

where ϵ_T is the brightness temperature noise and B is Planck radiance.

For GOES I/M the single channel noise was provided by Dr. Paul Menzel of NESDIS, as;

cm^{-1}	NEΔN $\left(mw/m^2.sr.^{cm^{-1}}\right)$	NEΔT*	cm^{-1}	NEΔN	NEΔT*	cm^{-1}	NEΔN	NEΔT*
680	0.9858	0.81	832	0.1416	0.13	2188	0.0089	0.42
696	0.7520	0.62	907	0.1032	0.10	2210	0.0069	0.35
711	0.6345	0.52	1030	0.1281	0.15	2245	0.0073	0.43
733	0.5090	0.42	1345	0.0675	0.17	2420	0.0031	0.37
748	0.4668	0.39	1425	0.0579	0.18	2513	0.0035	0.61
790	0.2266	0.20	1535	0.0891	0.40	2671	0.0014	0.47

*For 250°K

Total single channel noise $(\in)$ is comprised of instrument noise $(\in_I)$ and radiative transfer model error $(\in_m)$. A radiative transfer model forward error of 0.2K was assumed. Thus

$$\in = \sqrt{(\in_I * NF)^2 + \in_m^2}$$

where NF is a noise factor of 0.625, 0.286, 0.2, 0.1, and 0.05 as used throughout this study. Thus

$$\in_m \equiv 0.2\left(\frac{\partial B}{\partial T}\right)_{T_B}$$

348 GHIS channels used in this study are listed as follows:

Table IV: GHIS frequency used.

610.63	620.75	627.70	630.86	632.12	633.39	634.02	634.65	635.92	637.18
637.81	639.08	640.34	641.60	642.24	643.50	644.13	644.77	646.66	647.93
648.56	651.09	651.72	652.98	653.61	654.25	654.88	655.51	656.14	656.78
658.04	658.67	659.30	659.94	660.57	661.20	661.83	662.46	664.99	666.26
666.89	667.52	668.15	668.79	669.42	670.05	670.68	671.95	674.47	675.11
675.74	677.00	677.63	678.27	680.16	681.43	684.59	686.48	687.12	687.75
689.64	690.91	691.54	692.80	693.44	694.07	694.70	695.97	697.23	697.86
699.13	700.39	701.02	701.65	702.29	702.92	704.18	706.08	707.98	708.61
709.87	710.50	711.14	711.77	714.93	717.46	718.09	726.94	733.26	733.89

734.52	737.68	738.32	740.84	744.64	747.80	749.69	750.96	753.49	755.38
756.65	757.91	758.54	773.71	781.93	784.46	790.15	791.41	792.04	792.68
794.57	795.84	800.89	805.95	807.21	811.01	816.06	821.12	838.82	847.04
847.67	867.90	903.29	918.46	927.95	935.53	941.85	950.07	958.92	965.87
972.82	979.15	1072.06	1084.07	1092.92	1097.35	1103.04	1109.36	1116.31	1123.26
1127.06	1133.38	1153.60	1157.40	1211.38	1221.49	1222.76	1227.81	1231.60	1234.13
1240.45	1246.78	1249.30	1250.57	1255.62	1258.15	1261.95	1269.53	1280.91	1291.02
1293.55	1302.40	1320.10	1325.16	1334.00	1335.27	1344.12	1345.38	1347.91	1349.18
1352.97	1366.87	1369.40	1370.67	1371.93	1374.46	1375.72	1376.99	1378.25	1379.52
1380.78	1382.04	1383.31	1384.57	1388.37	1389.63	1390.89	1392.16	1395.95	1397.21
1399.74	1401.01	1402.27	1403.54	1406.06	1407.33	1408.59	1409.86	1411.12	1412.39
1413.65	1414.91	1416.18	1419.97	1421.23	1425.03	1426.29	1427.56	1431.35	1432.61
1433.88	1437.67	1438.93	1440.20	1441.46	1442.73	1443.99	1445.25	1449.05	1450.31
1452.84	1460.42	1461.69	1466.75	1468.01	1469.27	1476.86	1478.12	1479.39	1481.92
1483.18	1484.44	1492.03	1493.29	1500.88	1502.14	1536.28	1547.65	1551.45	1562.82
1572.94	1581.79	1586.84	1588.11	1598.22	1599.49	1624.77	1632.36	1658.90	1663.96
1665.22	1666.49	1672.81	1691.77	1693.04	1708.21	1710.74	1720.85	1722.11	1724.64
1725.91	1727.17	1728.43	1741.08	2177.93	2182.98	2190.57	2215.85	2223.44	2236.08
2238.61	2241.14	2243.66	2246.19	2248.72	2251.25	2256.31	2258.83	2261.36	2266.42
2281.59	2284.12	2286.65	2291.70	2296.76	2301.82	2306.87	2309.40	2311.93	2316.99
2319.52	2322.04	2324.57	2327.10	2329.63	2332.16	2334.69	2337.21	2339.74	2342.27
2344.80	2347.33	2349.86	2352.39	2354.91	2357.44	2359.97	2362.50	2365.03	2367.56
2370.08	2372.61	2375.14	2377.67	2380.20	2382.73	2385.25	2387.78	2390.31	2392.84
2395.37	2397.90	2400.42	2435.82	2453.52	2539.49	2559.71	2600.17	2605.22	2610.28
2615.34	2617.87	2622.92	2630.51	2633.04	2638.09	2640.62	2643.15	2645.68	2648.21
2650.74	2653.26	2668.43	2670.96	2686.13	2698.78	2701.30	2703.83		

References

Chedin, A., N. A. Scott, C. Wahiche, P. Moulinier, 1985: The Improved Initialization INversion method: a high resolution physical method for temperature retrievals from satellites of the TIROS-N series. J. Clim. Appl. Meteor., Vol. 24, 128-143.

Phillips, N., J. Susskind, L. McMillin, 1988: Results of a Joint NOAA/NASA Sounder Simulation Study. J. Atmos. & Ocean. Tech., Vol. 5(1), 44-56.

Rogers, C. D., 1976: Retrieval of atmospheric temperature and composition from remote measurements of thermal radiation. Rev. Geophys. and Space Phys., Vol. 14, 609-624.

Smith, W. L. and H. M. Woolf, 1976: The use of eigenvectors of statistical covariance matrices for interpreting satellite sounding radiometer observations. J. Atmos. Sci., Vol. 33, 1127-1140.

Table II: Root Mean Square Errors (RMSE) of retrieved temperatures and dewpoints within the 100-1000 hectapascal layer of the atmosphere. The RMSE's are presented as a function of instrument noise and vertical resolution.

Figure 1a: Temperature retrieval RMSE's for GHIS at various vertical resolutions as a function of instrument noise

Figure 1b: Same as **1a** but for GOES filter sounder.

Figure 2a: GHIS temperature retrieval RMSE as a function of vertical resolution for nominal noise (noise condition C2).

Figure 2b: Same as **2a** but for GOES filter radiometer.

Figure 3a: Comparison of GHIS and GOES filter radiometer temperature profile errors for nominal noise (noise condition C2) and a 2 kilometer vertical resolution.

Figure 3b: Same as **3a** but for dewpoint temperature.

Figure 4: An example comparison of GHIS and GOES filter radiometer temperature and dewpoint temperature retrievals as compared to the radiosonde used to simulate the radiance observations for each instrument.